ACS Macro Letters

pubs.acs.org/macroletters Letter

# Equilibrium Conformation of Catenated DNA Networks in Slitlike Confinement

Beatrice W. Soh and Patrick S. Doyle*

Cite This: *ACS Macro Lett.* 2021, 10, 880–885 Read Online

ACCESS | Metrics & More | Article Recommendations | Supporting Information

**ABSTRACT:** A kinetoplast is a planar network of catenated DNA rings with topology that resembles that of chain mail armor. In this work, we use single-molecule experiments to probe the conformation of kinetoplasts confined to slits. We find that the in-plane size of kinetoplasts increases with degree of confinement, akin to the slitlike confinement of linear DNA. The change in kinetoplast size with channel height is consistent with the scaling prediction from a Flory-type approach for a 2D polymer. With an increase in extent of confinement, the kinetoplasts appear to unfold and take on more uniform circular shapes, in contrast to the broad range of conformations observed for kinetoplasts in bulk.

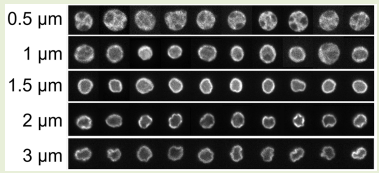




A fundamental understanding of how polymers behave in confinement is an area of scientific interest with significance in a broad range of contexts. From a polymer physics perspective, it is well-known that polymers exhibit markedly different properties in confined geometries than in bulk.[1] From a practical standpoint, the study of confined polymers has implications for fields ranging from polymer crystallization[2,3] to polymer nanocomposites.[4,5]

Since the emergence of single-molecule experiments about three decades ago as a tool to examine polymers on the molecular level, double-stranded DNA has been widely investigated as a model polymer.[6,7] Concurrent advances in microfabrication techniques have enabled experimental investigations into DNA molecules in well-defined confined geometries.[8−12] Given the significant role of DNA in molecular biology, the probing of nanoconfined DNA molecules is further motivated by an understanding of various biological processes, such as DNA packaging in vivo,[13,14] and the development of next-generation genomic technologies, including genome mapping and nanopore sequencing.[15,16]

The conformation of a polymer in bulk is determined by a balance between entropic elasticity and excluded volume.[1] When a linear polymer chain with persistence length $p$ is confined to a geometry with at least one dimension $d$ smaller than the equilibrium size in bulk $R_{G,bulk}$, the polymer deforms to an extent dependent on the degree of confinement. Under moderate confinement (de Gennes regime), $R_{G,bulk} > d \gg p$, excluded volume interactions give rise to elongation of the polymer. The behavior of the confined polymer can be characterized using blob theory, with the chain being described as a string of self-avoiding blobs with diameter $d$.[17−19] As the channel dimension approaches the persistence length, the chain is rigid over length scales on the order of the confining dimension, and the interplay between confinement and chain stiffness dominates the physics. Under strong confinement (Odijk regime), $p \gg d$, any backfolding is energetically unfavorable, and the chain can be viewed as a series of deflection segments off the walls.[20]

The statics and dynamics of linear DNA in confinement have been widely studied using both experiments[8−12] and simulations.[21−23] There is recent interest in polymers with more complex topologies, such as knotted,[24−26] ring,[27−30] and branched polymers,[31−33] yet the behavior of DNA with complex topologies in confined geometries remains largely unexplored, especially from an experimental approach. In particular, the effect of confinement on the conformation of molecules with sheet-like structures is intriguing not only from a physics viewpoint but also for its relevance to confined self-assembly or polymerization of sheets.[34]

Recently, our group proposed the kinetoplast as a model system for the facile experimental study of two-dimensional (2D) catenated polymers.[35,36] A kinetoplast is a planar network of topologically interlocked circular DNA and bears resemblance to chain mail armor. The kinetoplast topology is a subset of the more general Olympic gels.[37] Kinetoplasts from the mitochondria of the trypanosomatid *Crithidia fasciculata* contain approximately 5000 minicircles (∼2.5 kbp) and 25 maxicircles (∼40 kbp).[38−40] The topological complexity of the kinetoplast arises from mechanical bonds in the network, yet each minicircle with a fully extended contour of ∼5 Kuhn lengths can represent an effective bond in a coarse-grained 2D polymer model.

In this work, we use single-molecule experiments to probe the conformation of kinetoplasts in slitlike confinement.

**Received:** May 5, 2021
**Accepted:** June 22, 2021




https://doi.org/10.1021/acsmacrolett.1c00299
*ACS Macro Lett.* 2021, 10, 880–885

Through the observation of kinetoplasts in channels of varying heights, we quantify the confinement effects on kinetoplast size and shape. Similar to linear polymers, the in-plane size of kinetoplasts increases monotonically in slitlike confinement. The change in size with channel height is consistent with the scaling prediction based on a generalized Flory approach for a 2D polymer. Surprisingly, as the degree of confinement increases, the kinetoplasts unfold, and the resulting shapes transition from being highly anisotropic to highly isotropic.

In bulk solution, kinetoplasts adopt the conformation of a cup-shaped sheet with ∼5 $\mu$m diameter and ∼3 $\mu$m thickness.[35] We observe a range of sizes and shapes in a given population of kinetoplasts at equilibrium,[35,36] attributable to the kinetoplasts being extracted at different stages of the replication cycle and the unique connectivities of the underlying structures.[38−40] In this study, experiments were conducted in straight channels 40 $\mu$m wide and ∼1 cm long, with heights $h$ ranging from 0.5 to 3 $\mu$m. Kinetoplast DNA from *Crithidia fasciculata* (TopoGEN) was stained with fluorescent dye YOYO-1 at a base pair to dye ratio of 8:1 and allowed to equilibrate overnight. Prior to experiments, the DNA solution was diluted into experimental buffer containing 4 vol % of $\beta$-mercaptoethanol and 0.1% 10 kDa polyvinylpyrrolidone in 0.5X tris-borate-EDTA (TBE) solution. Kinetoplasts were driven into the channel by electrophoresis and allowed to relax at equilibrium for ∼30 s before image acquisition. Each kinetoplast was observed for 1000 frames at a frame rate of 25 frames per second (40 s). For each channel height, averages were taken over all frames for each kinetoplast and ensembles containing 70−130 kinetoplasts. We used an inverted Zeiss Axiovert microscope with a 63X 1.4 NA oil-immersion objective to visualize molecules and recorded images using a Photometrics Prime 95B sCMOS camera. See the Supporting Information (SI) for additional experimental and image analysis details and representative images of kinetoplasts confined to different channel heights.

Figure 1 shows a montage of fluorescence images of kinetoplasts in channels of different heights (see Figure S1 for images in bulk), based on which we can make a few qualitative observations. First, as the channel height decreases and degree of confinement increases, the kinetoplasts generally increase in size and display less diverse conformations. Kinetoplasts in a 3 $\mu$m tall channel can form a wide range of shapes, whereas kinetoplasts in a 0.5 $\mu$m tall channel tend to be uniformly circular. Second, the fluorescence patterns of kinetoplasts differ across channel heights. Previous work from our group[35] noted that kinetoplasts in bulk display bright edges when visualized under fluorescence microscopy, likely due to the dense fibrils observed at the periphery of the network. This is also observed from the images of kinetoplasts for $h \geq 1$ $\mu$m. On the contrary, kinetoplasts in a 0.5 $\mu$m tall channel display a notably different fluorescence pattern, with the interiors of the molecules exhibiting patchiness in intensity. It appears that increasing confinement serves to gradually unfold kinetoplasts, with the kinetoplasts in 0.5 $\mu$m tall channels flattened into highly isotropic shapes and revealing symmetric, recurring motifs in the intensity patterns that we believe to be related to the intrinsic structure of the catenated network. While kinetoplasts in bulk appear to be heterogeneous, the homogeneity in shape and size upon strong confinement suggests systemic patterns in the underlying topologies. See Figure S2 for more images of kinetoplasts in 0.5 $\mu$m tall channels.

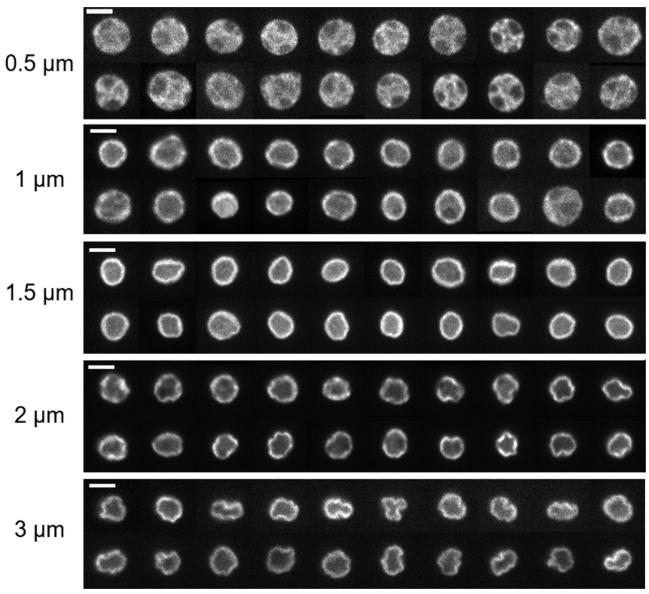


**Figure 1.** Images of different kinetoplasts in channels of different heights as labeled. Each image is a projection averaged over four frames. Scale bars represent 5 $\mu$m.

To quantify the size of kinetoplasts, we determine the major axis length ($L_M$), minor axis length ($L_m$), and radius of gyration ($R_G$) from the 2D projection of each kinetoplast. The major and minor axis lengths were calculated based on the eigenvalues of the radius of gyration tensor, and the radius of gyration was determined as the square root of the trace of the same tensor (see SI). As seen from Figure 2a, the mean in-plane $R_G$ of kinetoplasts increases with a decrease in channel height, similar to that observed for linear DNA in slitlike confinement.[9,10] Confining a polymer to a slit leads to a reduction in the dimension of the polymer in the channel height direction, which results in an increase in monomer density. The consequent increase in excluded-volume interactions causes the polymer to expand in the unconfined plane. We note that the mean $R_G$ does not vary much for $h > 1$ $\mu$m, compared to the differences in size upon further confinement at $h \leq 1$ $\mu$m. See the SI for discussion of kinetoplast size and shape fluctuations in time.

We can understand the quantitative change in kinetoplast size with channel height by developing a Flory-type scaling argument for a 2D polymer confined in a slit geometry. Given the strong self-avoidance of DNA, we expect the kinetoplasts to be in a flat phase.[41−43] This leads to a generalized Flory exponent of $\nu = 1$, and two-body interactions are determined to be mean-field relevant for the polymer system.[44,45] The conformation of a polymer is determined by a balance between the elastic and excluded volume interaction contributions to the free energy.[1] For a $D$-dimensional polymer in slitlike confinement, the Flory free energy is described by

$$\frac{F}{k_B T} \sim \frac{R_G^2}{N^{2-D} b^2} + \frac{v N^{2D}}{h R_G^2} \quad (1)$$

where $R_G$ is the size of the confined polymer; $N$ is the number of monomers in a given direction; $b$ is the Kuhn length; $v$ is the mean-field approximated excluded volume parameter; and $h$ is the slit height. Minimizing the free energy for $D = 2$, we arrive at the equilibrium size of the polymer, given by[46]


https://doi.org/10.1021/acsmacrolett.1c00299
ACS Macro Lett. 2021, 10, 880−885

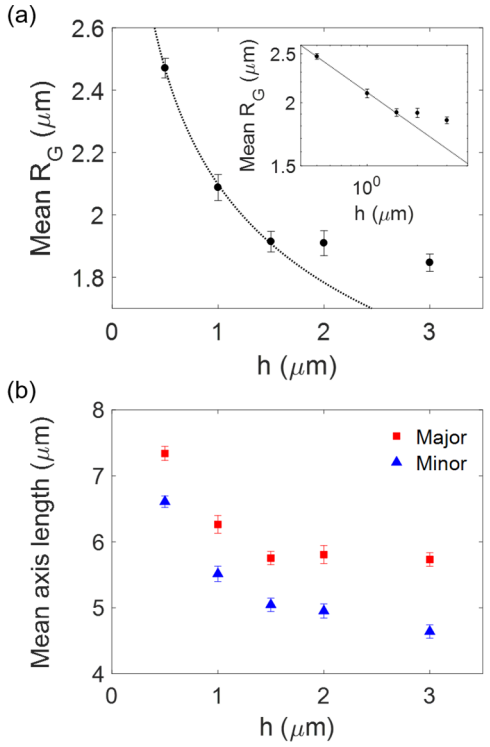


**Figure 2.** Ensemble average size of kinetoplasts. (a) Mean radius of gyration $R_G$ as a function of channel height $h$. Inset: same data shown on a log−log plot. The dotted lines represent a fit to $R_G = \alpha h^{\beta}$, yielding $\beta = -0.23 \pm 0.13$. (b) Mean major and minor axis lengths as a function of channel height. Error bars represent 95% confidence intervals.

$$R_G \sim \frac{\nu^{1/4} b^{1/2} N}{h^{1/4}} \tag{2}$$

We note that the scaling prediction $R_G \sim h^{-1/4}$ is the same as that for a linear polymer confined to a slit in the de Gennes regime.[1] Interestingly, a computational study on the confinement of star-branched, dendritic, and hyperbranched chains in slits has reported the scaling of in-plane size with confining dimension for the different topologies to be similar to that of linear chains.[47]

We point out several underlying assumptions of the Flory-type scaling argument presented. First, we make the simplifying assumption of uniform monomer density in a kinetoplast. The density of minicircles within the interior of a kinetoplast has been measured from electron microscopy images, and only a small variation was found between measurements at different locations across different molecules;[48] hence, we believe this to be a reasonable assumption. We acknowledge that this assumption might be challenged in the strong confinement regime, in which we begin to see distinct fluorescence patterns within the kinetoplast interior. However, we also note that because we use the Flory scaling argument to predict the largest measurable length scale, such nonidealities might be averaged out by the mean field approach. Second, we neglect any entropic contribution from the intramolecular topological constraints within each kinetoplast. This is supported by recent work demonstrating that the size of the overlap region of topologically linked rings adjusts to the blob size for all degrees of confinement and always remains much larger than the highly stretched limit.[49]

We fit the experimental data for $h < 2$ $\mu$m, over which there is a notable change in $R_G$, and obtain a scaling exponent of $-0.23 \pm 0.13$ (95% confidence interval). Remarkably, despite the simplified representation of the kinetoplast and mean-field approximation of the Flory approach, the data appear to follow the expected scaling prediction. We highlight that the choice to fit only the three data points that correspond to the smaller confinement heights is based on the notable difference in $R_G$ with change in channel height within this range. The lack of an appreciable change in kinetoplast size with channel height for $h \geq 2$ $\mu$m suggests that the kinetoplasts are in a transition regime approaching the unconfined regime, in which we might expect a different scaling exponent. Similarly, we cannot exclude that the scaling exponent will be different under stronger confinement beyond $h < 0.5$ $\mu$m. This will be interesting to investigate in further studies into the behavior of catenated polymers in more strongly confined regimes.

To gain further insight into the effects of confinement on kinetoplast size, we consider separately the change in major and minor axis lengths with channel height (Figure 2b). For $h \geq 1.5$ $\mu$m, the mean major axis length of kinetoplasts remains relatively constant, while the mean minor axis length shows an increase upon stronger confinement in the same region. This suggests that the initial response of kinetoplasts to confinement is expansion preferentially in the direction that affords the greatest degree of freedom, which also leads to the kinetoplasts

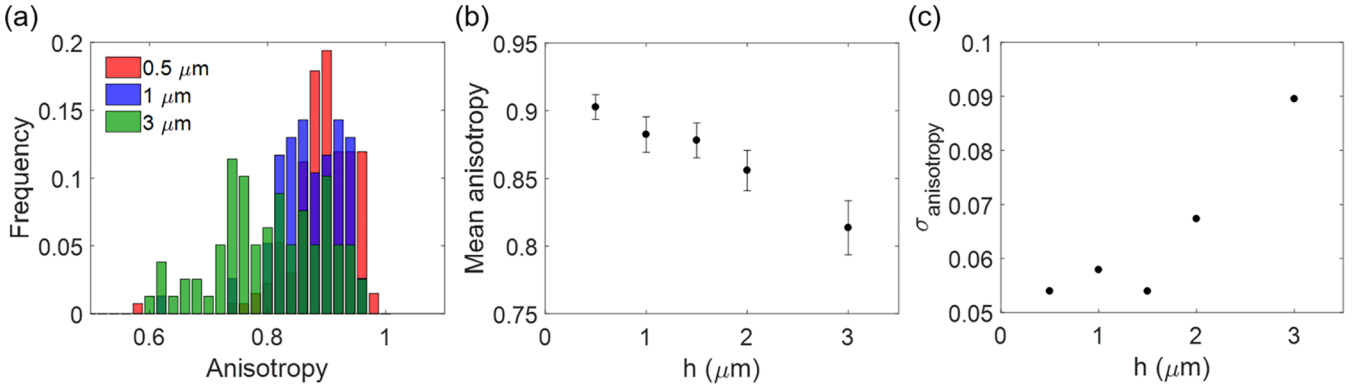


**Figure 3.** Anisotropy of kinetoplasts. (a) Histograms of anisotropy for ensembles of kinetoplasts in 0.5, 1, and 3 $\mu$m tall channels. (b) Mean anisotropy as a function of channel height. Error bars represent 95% confidence intervals. (c) Standard deviation in anisotropy as a function of channel height, reflecting the spread in anisotropy within each ensemble.



https://doi.org/10.1021/acsmacrolett.1c00299
ACS Macro Lett. 2021, 10, 880−885

becoming more isotropic. For $h < 1.5$ $\mu$m, both mean major and minor axis lengths increase dramatically with a decrease in channel height. The differential change in major axis length around $h = 1.5$ $\mu$m points to the onset of a different confinement regime, in which it becomes energetically more favorable to expand radially within the channel. Although moderate and strong confinement for linear DNA typically refers to the de Gennes and Odijk regimes, respectively, we highlight that the validity of such regimes for kinetoplasts is not yet known. Given the complex topology of the kinetoplast structure, we expect the same slit height to induce stronger confinement effects for kinetoplasts compared to linear DNA with an equivalent $R_{G,bulk}$. In this text, we use moderate confinement to refer to $h \geq 1.5$ $\mu$m and strong confinement for $h < 1.5$ $\mu$m.

We can gauge the relative contributions of the major and minor axis lengths to kinetoplast size by determining the anisotropy, defined as the ratio of minor to major axis length:

$$\text{anisotropy} = \frac{L_m}{L_M} \tag{3}$$

An anisotropy value of 0 represents a straight line, and an anisotropy value of 1 corresponds to a circular conformation. Figure 3a shows the distributions of anisotropy for ensembles of kinetoplasts in channels with $h = 0.5$, 1, and 3 $\mu$m. Despite some overlap between the distributions at different $h$, there is a distinct shift in anisotropies between $h = 0.5$ $\mu$m and $h = 3$ $\mu$m, with the kinetoplasts subjected to strong confinement also taking on a narrower range of anisotropy values. See the SI for distributions of major and minor axis lengths for the same ensembles. We plot the mean and standard deviation of the anisotropy values for the kinetoplasts as a function of $h$ (Figures 3b and c), with the standard deviation reflecting the spread in anisotropy across an ensemble. As the channel height decreases, the mean anisotropy increases, and the standard deviation in anisotropy decreases, indicating that the kinetoplasts become more isotropic and uniformly shaped with greater confinement. The increase in mean anisotropy is larger for moderate confinement compared to strong confinement. This is in alignment with the crossover point at which the major axis length also changes in response to confinement, but the monotonic increase in mean anisotropy with increased confinement reveals that the change in minor axis length with confinement is always proportionally larger than the concurrent change in major axis length. We point out that the distributions of anisotropy are broad and even for linear DNA confined to a slit with height approximately equal to the Kuhn length,[9] in contrast to the histogram shapes for kinetoplasts under strong confinement. This is due to the additional degree of freedom afforded to linear (1D) polymers versus 2D polymers, which allows for exploration of the two-dimensional space when confined to a slit and adoption of a variety of shapes.

The variation in kinetoplast shapes at different extents of confinement can be examined in greater detail by extracting and comparing the outlines of kinetoplasts between different ensembles. We use the Chan−Vese active contour algorithm[50] to determine the outline of each kinetoplast, the polar coordinates of which are described by 72 points separated by 5 degrees each, and employ principal component analysis (PCA) to characterize the shape variation of kinetoplasts confined to different channel heights. By examining the principal components ordered by decreasing variance (Figure 4a), we identify the modes that account for the greatest variance in each ensemble. We highlight that the principal

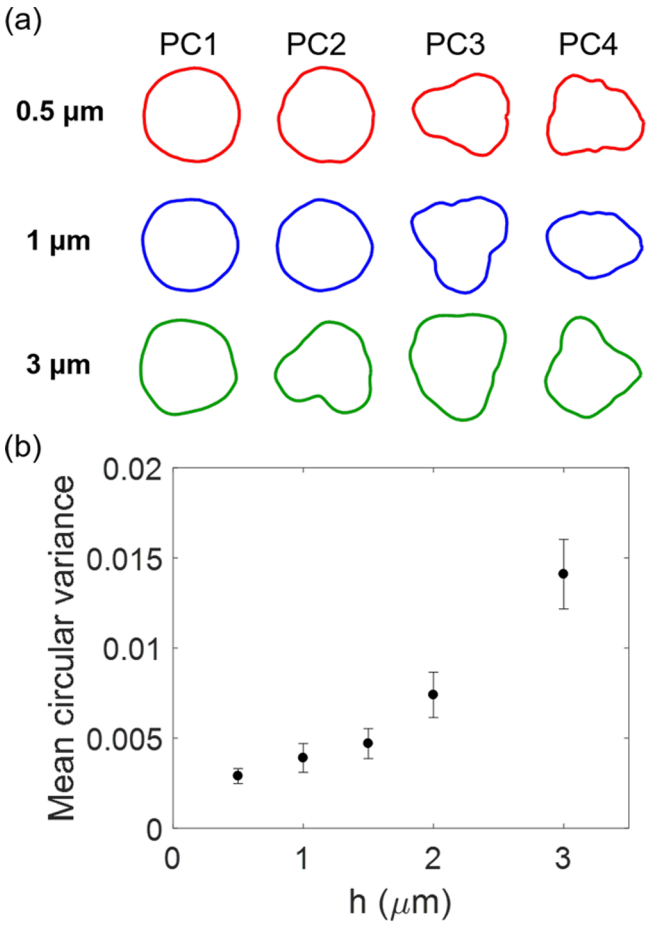


**Figure 4.** (a) Images of the first four principal components obtained from principal component analysis of kinetoplast outlines for kinetoplasts in 0.5, 1, and 3 $\mu$m tall channels. (b) Mean circular variance of kinetoplasts as a function of channel height. Error bars represent 95% confidence intervals.

component modes shown in Figure 4a reflect the variations in kinetoplast shapes and are represented as radial modulations with respect to an arbitrary reference circle. Across all channel heights, the main modes of shape variation, which correspond to the first principal components, are described by circular shapes. For $h = 0.5$ $\mu$m and $h = 1$ $\mu$m, the second modes are also circular in shape, whereas for $h = 3$ $\mu$m, the second mode can be described as being heart-shaped. This is consistent with the observation that kinetoplasts under moderate confinement can exhibit shapes with complex edge curvature,[35] while kinetoplasts subjected to strong confinement tend to take on more circular shapes (Figure 1). See SI for details on PCA and further analysis.

We quantify the extent to which the kinetoplasts in each ensemble can be described by a circular shape using the shape descriptor circular variance, defined as[51]

$$\text{circular variance} = \frac{1}{N\mu_r^2}\sum_i (\|\mathbf{s_i} - \boldsymbol{\mu}\| - \mu_r)^2 \tag{4}$$

where $\mathbf{s} = \{\mathbf{s_i}\}$ is the set of $N$ points describing the kinetoplast outline; $\boldsymbol{\mu} = \frac{1}{N}\sum_i \mathbf{s_i}$ is the centroid; and $\mu_r = \frac{1}{N}\sum_i \| \mathbf{s_i} - \boldsymbol{\mu} \|$


https://doi.org/10.1021/acsmacrolett.1c00299
ACS Macro Lett. 2021, 10, 880−885

is the mean radius. The circular variance is the scaled mean squared error with respect to a solid circle; hence, a perfect circle has a circular variance of zero. Figure 4b shows the mean circular variance of kinetoplast outlines as a function of channel height. In accordance with observations based on Figure 1, the mean circular variance decreases monotonically with an increase in degree of confinement, showing that the kinetoplasts become increasingly circular upon stronger confinement.

While kinetoplasts in bulk and moderate confinement can adopt a wide variety of conformations that remain persistent over long observation times,[35] kinetoplasts under strong confinement form highly isotropic, circular shapes. The uniformity of the flattened quasi-2D shapes informs us that the intrinsic conformations of the kinetoplasts are similar in terms of overall connectivity, yet the presence of long-lived buckled shapes in bulk and moderate confinement that vary from molecule to molecule suggests that there are differences in the bending energetics that give rise to unique conformations. It is unclear at this point in time if the differences in bending energetics arise from local variations in the density of the minicircles or the topology of the maxicircles. This poses an interesting problem for potential investigation using simulations.[52,53]

In this work, we studied the conformation of kinetoplasts confined in slits. Similar to linear DNA, the in-plane $R_G$ of kinetoplasts increases in slitlike confinement, and the quantitative change in size can be rationalized by a Flory-type scaling argument for a 2D polymer. The nonlinear topology of the kinetoplast gives rise to rich shape behavior, with the highly anisotropic kinetoplasts becoming highly isotropic as the extent of confinement increases. Our findings show similarities between confined linear polymers and kinetoplasts but also demonstrate the unexpected effects that stem from the complex catenated structure of the kinetoplast.

## ■ ASSOCIATED CONTENT

### Supporting Information

The Supporting Information is available free of charge at https://pubs.acs.org/doi/10.1021/acsmacrolett.1c00299.

> Representative movies of kinetoplasts confined to different channel heights, details about experimental protocol and image analysis, additional images of kinetoplasts, kinetoplast size and shape fluctuations in time, power-law fit to kinetoplast size across all channel heights, distributions of major and minor axis lengths for various ensembles, and details about PCA analysis (PDF)

## ■ AUTHOR INFORMATION


### Corresponding Author

**Patrick S. Doyle** − *Department of Chemical Engineering, Massachusetts Institute of Technology, Cambridge, Massachusetts 02139, United States;* orcid.org/0000-0003-2147-9172; Email: pdoyle@mit.edu

### Author

**Beatrice W. Soh** − *Department of Chemical Engineering, Massachusetts Institute of Technology, Cambridge, Massachusetts 02139, United States;* Present Address: Institute of Materials Research and Engineering, 2 Fusionopolis Way, Singapore 138634; orcid.org/0000-0001-8399-5995

Complete contact information is available at: https://pubs.acs.org/10.1021/acsmacrolett.1c00299


### Notes

The authors declare no competing financial interest.

## ■ ACKNOWLEDGMENTS

This work was supported by the National Science Foundation (NSF) grant CBET-1936696. B.W.S. is funded by the Agency for Science, Technology and Research (A*STAR), Singapore.

## ■ REFERENCES


(1) Rubinstein, M.; Colby, R. H. *Polymer Physics*; Oxford University Press, 2003.

(2) Carr, J. M.; Langhe, D. S.; Ponting, M. T.; Hiltner, A.; Baer, E. Confined Crystallization in Polymer Nanolayered Films: A Review. *J. Mater. Res.* **2012**, *27* (10), 1326−1350.

(3) Michell, R. M.; Müller, A. J. Confined Crystallization of Polymeric Materials. *Prog. Polym. Sci.* **2016**, *54*−*55*, 183−213.

(4) Rittigstein, P.; Priestley, R. D.; Broadbelt, L. J.; Torkelson, J. M. Model Polymer Nanocomposites Provide an Understanding of Confinement Effects in Real Nanocomposites. *Nat. Mater.* **2007**, *6* (4), 278−282.

(5) Richter, D.; Kruteva, M. Polymer Dynamics Under Confinement. *Soft Matter* **2019**, *15* (37), 7316−7349.

(6) Shaqfeh, E. S. G. The Dynamics of Single-Molecule DNA in Flow. *J. Non-Newtonian Fluid Mech.* **2005**, *130* (1), 1−28.

(7) Schroeder, C. M. Single Polymer Dynamics for Molecular Rheology. *J. Rheol.* **2018**, *62* (1), 371−403.

(8) Maier, B.; Rädler, J. O. DNA on Fluid Membranes: A Model Polymer in Two Dimensions. *Macromolecules* **2000**, *33*, 7185−7194.

(9) Lin, P. K.; Fu, C. C.; Chen, Y. L.; Chen, Y. R.; Wei, P. K.; Kuan, C. H.; Fann, W. S. Static Conformation and Dynamics of Single DNA Molecules Confined in Nanoslits. *Phys. Rev. E* **2007**, *76* (1), 011806.

(10) Tang, J.; Levy, S. L.; Trahan, D. W.; Jones, J. J.; Craighead, H. G.; Doyle, P. S. Revisiting the Conformation and Dynamics of DNA in Slitlike Confinement. *Macromolecules* **2010**, *43* (17), 7368−7377.

(11) Reisner, W.; Morton, K. J.; Riehn, R.; Wang, Y. M.; Yu, Z.; Rosen, M.; Sturm, J. C.; Chou, S. Y.; Frey, E.; Austin, R. H. Statics and Dynamics of Single DNA Molecules Confined in Nanochannels. *Phys. Rev. Lett.* **2005**, DOI: 10.1103/PhysRevLett.94.196101.

(12) Stein, D.; Van Der Heyden, F. H. J.; Koopmans, W. J. A.; Dekker, C. Pressure-Driven Transport of Confined DNA Polymers in Fluidic Channels. *Proc. Natl. Acad. Sci. U. S. A.* **2006**, *103* (43), 15853−15858.

(13) Marenduzzo, D.; Micheletti, C.; Orlandini, E. Biopolymer Organization Upon Confinement. *J. Phys.: Condens. Matter* **2010**, *22* (28), 283102.

(14) Smith, D. E. Single-Molecule Studies of Viral DNA Packaging. *Curr. Opin. Virol.* **2011**, *1* (2), 134−141.

(15) Levy, S. L.; Craighead, H. G. DNA Manipulation, Sorting, and Mapping in Nanofluidic Systems. *Chem. Soc. Rev.* **2010**, *39* (3), 1133−1152.

(16) Reisner, W.; Pedersen, J. N.; Austin, R. H. DNA Confinement in Nanochannels: Physics and Biological Applications. *Rep. Prog. Phys.* **2012**, *75* (10), 106601.

(17) Daoud, M.; De Gennes, P. G. Statistics of Macromolecular Solutions Trapped in Small Pores. *J. Phys. (Paris)* **1977**, *38* (1), 85−93.

(18) Brochard, F. Dynamics of Polymer Chains Trapped in a Slit. *J. Phys. (Paris)* **1977**, *38* (10), 1285−1291.

(19) Brochard, F.; De Gennes, P. G. Dynamics of Confined Polymer Chains. *J. Chem. Phys.* **1977**, *67* (1), 52−56.

(20) Odijk, T. On the Statistics and Dynamics of Confined or Entangled Stiff Polymers. *Macromolecules* **1983**, *16* (8), 1340−1344.

(21) Jendrejack, R. M.; Schwartz, D. C.; Graham, M. D.; De Pablo, J. J. Effect of Confinement on DNA Dynamics in Microfluidic Devices. *J. Chem. Phys.* **2003**, *119* (2), 1165−1173.
(22) Cifra, P. Channel Confinement of Flexible and Semiflexible Macromolecules. *J. Chem. Phys.* **2009**, *131* (22), 224903.
(23) Wang, Y.; Tree, D. R.; Dorfman, K. D. Simulation of DNA Extension in Nanochannels. *Macromolecules* **2011**, *44* (16), 6594−6604.
(24) Saitta, A. M.; Soper, P. D.; Wasserman, E.; Klein, M. L. Influence of a Knot on the Strength of a Polymer Strand. *Nature* **1999**, *399*, 46−48.
(25) Caraglio, M.; Micheletti, C.; Orlandini, E. Stretching Response of Knotted and Unknotted Polymer Chains. *Phys. Rev. Lett.* **2015**, *115* (18), 188301.
(26) Soh, B. W.; Narsimhan, V.; Klotz, A. R.; Doyle, P. S. Knots Modify the Coil-Stretch Transition in Linear DNA Polymers. *Soft Matter* **2018**, *14*, 1689−1698.
(27) Robertson, R. M.; Laib, S.; Smith, D. E. Diffusion of Isolated DNA Molecules: Dependence on Length and Topology. *Proc. Natl. Acad. Sci. U. S. A.* **2006**, *103* (19), 7310−4.
(28) Li, Y.; Hsiao, K. W.; Brockman, C. A.; Yates, D. Y.; Robertson-Anderson, R. M.; Kornfield, J. A.; San Francisco, M. J.; Schroeder, C. M.; McKenna, G. B. When Ends Meet: Circular DNA Stretches Differently in Elongational Flows. *Macromolecules* **2015**, *48* (16), 5997−6001.
(29) Tsalikis, D. G.; Mavrantzas, V. G.; Vlassopoulos, D. Analysis of Slow Modes in Ring Polymers: Threading of Rings Controls Long-Time Relaxation. *ACS Macro Lett.* **2016**, *5* (6), 755−760.
(30) Soh, B. W.; Klotz, A. R.; Robertson-Anderson, R. M.; Doyle, P. S. Long-Lived Self-Entanglements in Ring Polymers. *Phys. Rev. Lett.* **2019**, *123* (4), 048002.
(31) Heuer, D. M.; Saha, S.; Archer, L. A. Electrophoretic Dynamics of Large DNA Stars in Polymer Solutions and Gels. *Electrophoresis* **2003**, *24* (19−20), 3314−3322.
(32) Mai, D. J.; Schroeder, C. M. Single Polymer Dynamics of Topologically Complex DNA. *Curr. Opin. Colloid Interface Sci.* **2016**, *26* (28−40), 28.
(33) Mai, D. J.; Saadat, A.; Khomami, B.; Schroeder, C. M. Stretching Dynamics of Single Comb Polymers in Extensional Flow. *Macromolecules* **2018**, *51* (4), 1507−1517.
(34) Zhuang, X.; Mai, Y.; Wu, D.; Zhang, F.; Feng, X. Two-Dimensional Soft Nanomaterials: A Fascinating World of Materials. *Adv. Mater.* **2015**, *27* (3), 403−427.
(35) Klotz, A. R.; Soh, B. W.; Doyle, P. S. Equilibrium Structure and Deformation Response of 2D Kinetoplast Sheets. *Proc. Natl. Acad. Sci. U. S. A.* **2020**, *117* (1), 121−127.
(36) Soh, B. W.; Doyle, P. S. Deformation Response of Catenated DNA Networks in a Planar Elongational Field. *ACS Macro Lett.* **2020**, *9*, 944−949.
(37) Krajina, B. A.; Zhu, A.; Heilshorn, S. C.; Spakowitz, A. J. Active DNA Olympic Hydrogels Driven by Topoisomerase Activity. *Phys. Rev. Lett.* **2018**, DOI: 10.1103/PhysRevLett.121.148001.
(38) Shapiro, T. A.; Englund, P. T. The Structure and Replication of Kinetoplast DNA. *Annu. Rev. Microbiol.* **1995**, *49* (1), 117−143.
(39) Liu, B.; Liu, Y.; Motyka, S. A.; Agbo, E. E. C.; Englund, P. T. Fellowship of the Rings: The Replication of Kinetoplast DNA. *Trends Parasitol.* **2005**, *21* (8), 363−369.
(40) Jensen, R. E.; Englund, P. T. Network News: The Replication of Kinetoplast DNA. *Annu. Rev. Microbiol.* **2012**, *66* (1), 473−491.
(41) Plischke, M.; Boal, D. Absence of a Crumpling Transition in Strongly Self-Avoiding Tethered Membranes. *Phys. Rev. A: At., Mol., Opt. Phys.* **1988**, *38* (9), 4943−4945.
(42) Abraham, F. F.; Rudge, W. E.; Plischke, M. Molecular Dynamics of Tethered Membranes. *Phys. Rev. Lett.* **1989**, *62* (15), 1757−1759.
(43) Kantor, Y.; Kremer, K. Excluded-Volume Interactions in Tethered Membranes. *Phys. Rev. E: Stat. Phys., Plasmas, Fluids, Relat. Interdiscip. Top.* **1993**, *48* (4), 2490−2497.
(44) Cates, M. E. Statics and Dynamics of Polymeric Fractals. *Phys. Rev. Lett.* **1984**, *53* (9), 926−929.
(45) Schlüter, A. D.; Payamyar, P.; Öttinger, H. C. How the World Changes By Going from One- to Two-Dimensional Polymers in Solution. *Macromol. Rapid Commun.* **2016**, *37* (20), 1638−1650.
(46) Soh, B. W.; Khorshid, A.; Al Sulaiman, D.; Doyle, P. S. Ionic Effects on the Equilibrium Conformation of Catenated DNA Networks. *Macromolecules* **2020**, *53* (19), 8502−8508.
(47) Chen, Z.; Escobedo, F. A. Conformational Properties and Entropic Partitioning of Topologically Complex Polymers Under Confinement. *Macromolecules* **2001**, *34* (25), 8802−8810.
(48) Chen, J.; Englund, P. T.; Cozzarelli, N. R. Changes in Network Topology During the Replication of Kinetoplast DNA. *EMBO J.* **1995**, *14* (24), 6339−6347.
(49) Amici, G.; Caraglio, M.; Orlandini, E.; Micheletti, C. Topologically Linked Chains in Confinement. *ACS Macro Lett.* **2019**, *8* (4), 442−446.
(50) Chan, T. F.; Vese, L. A. Active Contours Without Edges. *IEEE Transactions on Image Processing* **2001**, *10* (2), 266−277.
(51) Peura, M.; Iivarinen, J. Efficiency of Simple Shape Descriptors. In *Advances in Visual Form Analysis*; World Scientific, 1997; pp 443−451.
(52) Michieletto, D. A Bio-Physical Model for the Kinetoplast DNA. In *Topological Interactions in Ring Polymers*; Springer, 2016; pp 79−94.
(53) Rauscher, P. M.; Rowan, S. J.; de Pablo, J. J. Hydrodynamic Interactions in Topologically Linked Ring Polymers. *Phys. Rev. E: Stat. Phys., Plasmas, Fluids, Relat. Interdiscip. Top.* **2020**, *102*, 032502.


https://doi.org/10.1021/acsmacrolett.1c00299
*ACS Macro Lett.* 2021, 10, 880−885